including any outermost stable layer. We achieved an equilibrium state by balancing the Reynolds stress of the penetrative convection rolls against the viscous shear of the mean zonal flow. The alternately directed jets of the mean zonal wind may be a result of additional instabilities when the mean flow $\overline{\mathbf{V}}$ is strong, as suggested by three-dimensional numerical simulations (*29*). Because penetrative convection inside the cylinder tangent to the inner sphere's equator requires a much larger temperature gradient to excite, the zonal flow structure in lower latitudes $\phi < 45°$ (determined from the size of the metallic inner core) is fundamentally different from that in higher latitudes. The confinement of the zonal flow jets to the equatorial regions outside the tangent cylinder suggests a rotationally dominated deep convection origin (*15*). Furthermore, the jovian zonal jets are roughly symmetric about the equator and appear to be rather stable, indicating that they are controlled by rotation and deep convection with a long time scale. As a consequence of rapid rotation and spherical geometry, deep convection can readily penetrate through the entire H-He envelope and produce a mean zonal wind with an amplitude that can be much larger than that of the corresponding nonaxisymmetric (eddy) convective flows. Our results on penetrative spherical rotating convection have implications for the dynamics of Earth's fluid core and the sun's convection zone, places where there may be stably stratified layers (*30*, *31*).

REFERENCES AND NOTES

1. D. H. Atkinson, J. B. Pollack, A. Seiff, *Science* **272**, 842 (1996).
2. P. J. Gierasch and B. J. Conrath, *J. Geophys. Res.* **98**, 5459 (1993).
3. T. Guillot, D. Gautier, G. Chabrier, B. Mosser, *Icarus* **112**, 337 (1994).
4. T. Guillot, G. Chabrier, P. Morel, D. Gautier, *ibid.*, p. 354.
5. W. B. Hubbard, *Astrophys. J.* **152**, 745 (1968).
6. H. K. Moffatt, *Magnetic Field Generation in Electrically Conducting Fluids* (Cambridge Univ. Press, Cambridge, 1978).
7. D. J. Stevenson and E. E. Salpeter, *Astrophys. J. Suppl. Ser.* **35**, 221 (1977).
8. A. Seiff *et al.*, *Science* **272**, 844 (1996).
9. A. D. DelGenio and K. B. McGrattan, *Icarus* **84**, 29 (1990).
10. B. Straughan, *Mathematical Aspects of Penetrative Convection* (Longman Scientific and Technical, London, 1993).
11. G. Veronis, *Astrophys. J.* **137**, 641 (1963).
12. P. C. Matthews, *J. Fluid Mech.* **188**, 571 (1988).
13. F. H. Busse, *ibid.* **44**, 441 (1970).
14. K. Zhang, *ibid.* **236**, 535 (1992).
15. F. H. Busse, *Icarus* **29**, 255 (1976).
16. ———, *Astrophys. J.* **159**, 620 (1970).
17. Z.-P. Sun, G. Schubert, G. A. Glatzmaier, *Science* **260**, 661 (1993).
18. G. A. Glatzmaier and P. Olson, *Geophys. Astrophys. Fluid Dyn.* **70**, 113 (1993).
19. J. B. Manneville and P. Olson, *Icarus*, in press.
20. F. H. Busse and L. Hood, *Geophys. Astrophys. Fluid Dyn.* **21**, 59 (1981).
21. R. L. Kirk and D. J. Stevenson, *Astrophys. J.* **316**, 836 (1987).
22. Take the typical mean flow speed $V_0 = O(100$ m $s^{-1})$, $\nu = 10^{-6}$ m^2 s^{-1}, $L = O(10^7$ m), and $\Omega = 1.76 \times 10^{-4}$ s^{-1} [see, for example, (*7*) and F. M. Flaser, *Icarus* **26**, 280 (1986)].
23. A Boussinesq fluid spherical shell of constant thermal diffusivity κ, constant thermal expansion coefficient α, and constant viscosity ν that is rotating uniformly with a constant angular velocity Ω was assumed. Stress-free and isothermal boundary conditions were also assumed.
24. We have concentrated on the case with the ratio of the inner to outer radius $r_i/r_O = 0.35$. Solutions with other values of r_i/r_O were obtained and show similar features. In our calculation, E is based on the thickness of the shell, $E = \nu/2(r_O - r_i)^2\Omega$.
25. We have used a temperature gradient of the form

$$\frac{dT}{dr} = \frac{3r^*\mathcal{T}}{(n+3)(r_o - r_i)}\left[(r^*)^n - \left(\frac{\beta r_o^*}{r^*}\right)^3\right]$$

where $r^* = r/(r_O - r_i)$ and n, $\mathcal{T}$, and β are parameters. We have focused on the case with $n = 0$ and $\beta = 0.6$. Convection takes place when the Rayleigh number $R = \alpha\mathcal{T}\, g(r_O - r_i)^4/(\kappa\nu)$ is sufficiently large, where g is the acceleration due to gravity; $\mathcal{T}$ measures the magnitude of the driving temperature gradient in the model and determines the vigor of convection through R. The model only qualitatively simulates conditions in the "real" Jupiter.
26. A. P. Ingersoll *et al.*, *J. Geophys. Res.* **86**, 8733 (1981).
27. The linearized Navier-Stokes equation and the heat equation for penetrative convection in a rotating spherical shell are solved. The heat equation is solved analytically in terms of Bessel functions whereas the Navier-Stokes equation is solved numerically by the spectral method.
28. $\tilde{R}_e = (D|\mathbf{V}|_t)/\nu$, where D is the typical length scale of convective eddies. Take $D|\mathbf{V}|_t) = O(10^3$ m^2 s$^{-1})$ [B. Fegley and K. Lodders, *Icarus* **110**, 117 (1994)] and $\nu = 10^{-6}$ m^2 s^{-1} (*7*), we obtain $\tilde{R}_e\eta_i \gg 1$ for a moderate value of η_i.
29. Z.-P. Sun and G. Schubert, *Phys Fluids* **7**, 2686 (1995).
30. J. A. Jacobs, *The Earth's Core* (Academic Press, New York, 1975).
31. J. P. Zahn, in *Lecture Notes in Physics*, D. Gough and J. Toomre, Eds. (Springer-Verlag, Berlin, 1990), vol. 388, pp. 225–232.

32. The work of K.Z. was supported by the Institute of Geophysics and Planetary Physics, University of California, Los Angeles.

18 April 1996; accepted 3 July 1996

An Archean Geomagnetic Reversal in the Kaap Valley Pluton, South Africa

Paul W. Layer,* Alfred Kröner, Michael McWilliams

The Kaap Valley pluton in South Africa is a tonalite intrusion associated with the Archean Barberton Greenstone Belt. Antipodal paleomagnetic directions determined from the central and marginal parts of the pluton record a geomagnetic reversal that occurred as the pluton cooled. The age of the reversal is constrained by an $^{40}Ar/^{39}Ar$ plateau age from hornblende at 3214 ± 4 million years, making it the oldest known reversal. The data presented here suggest that Earth has had a reversing, perhaps dipolar, magnetic field since at least 3.2 billion years ago.

The behavior of Earth's magnetic field is preserved in the geologic record and can be deciphered with paleomagnetic techniques. With these techniques one can determine the location of the magnetic pole relative to the rock unit at the time the rock cooled through its magnetic blocking temperature. Knowledge of ancient pole positions and magnetic polarities has been used to construct models of plate motion (supercontinent positions and plate velocities) and the geomagnetic dynamo (reversal frequency and intensity). The usefulness of any paleomagnetic pole is determined by the stability of its magnetization (as determined by, for example, stepwise demagnetization, reversal tests, fold tests, or contact tests) and the ability to determine the time when magnetization was acquired. Few records of Earth's geomagnetic field from before 3 billion years ago (Ga) exist. Two early Archean paleopole positions for rocks as old as 3.45 Ga have been reported (*1*), but each study yielded only unipolar directions, with few stability tests. Here, we used paleomagnetic techniques to investigate an Archean tonalite pluton, and our results, when coupled with the results of a detailed geochronologic study (*2*), indicate a 3.2-Ga paleomagnetic pole constrained by reversal and contact tests. Well-documented and dated paleopoles are necessary to construct apparent polar-wander paths, and from these poles minimum average Archean plate velocities can be calculated (*3*).

The Kaap Valley pluton is a circular intrusion 30 km in diameter that forms a valley surrounded by the more mountainous Barberton Greenstone Belt to the north, east, and south (Fig. 1). It is overlain to the west by the early Proterozoic Transvaal Supergroup. The Transvaal Supergroup and related rocks form a thick sequence with an age range from 2552 ± 11 million years ago (Ma) at the base to 2432 ± 31 Ma near the

P. W. Layer, Geophysical Institute, University of Alaska, Fairbanks, AK 99775, USA.
A. Kröner, Institut für Geowissenschaften, Johannes Gutenburg-Universität, 55099 Mainz, Germany.
M. McWilliams, Department of Geophysics, Stanford University, Stanford, CA 94305, USA.
*To whom correspondence should be addressed.

top of the sequence (4). The main part of the Kaap Valley pluton is composed of hornblende-biotite tonalite, and the southeast margin and several isolated areas are composed of hornblende tonalite with little or no biotite (5). Pluton emplacement has been dated at 3226 ± 4 Ma (2, 6) by U-Pb dating of zircon, and there is no significant age difference between the interior and the margin of the intrusion. Hornblende samples from the interior and the margin have $^{40}Ar/^{39}Ar$ plateau ages of 3214 ± 4 Ma, determined by single-grain laser step-heating (2). The 13–million year age difference between the zircon and hornblende ages may reflect cooling that occurred after intrusion of the pluton. Biotite from the interior has a plateau age of 3142 ± 20 Ma (2). This age also reflects slow pluton cooling after intrusion and indicates that the pluton has not been subjected to any regional reheating event above ~250°C, which could have reset the magnetization since that time.

Within the Kaap Valley pluton, 323 oriented core samples were collected for paleomagnetic study from 46 sites. Twelve samples were from dolerite dikes of presumed early Proterozoic age (predicted on the basis of crosscutting relations) that pervasively cut the Kaap Valley pluton with a general northwest trend. In addition, 28 samples were collected from seven sites in folded shale units of the Moodies Group near its contact with the pluton (Fig. 1). The Moodies Group is the youngest stratigraphic unit of the Barberton Greenstone Belt.

One specimen core from each of the tonalite and dike samples was stepwise demagnetized in alternating fields (AFs) up to 80 mT. One specimen core from the shale samples was stepwise thermally demagnetized up to 700°C. Second specimen cores from all dike and selected tonalite samples were also thermally demagnetized, and selected shale samples were AF-demagnetized to determine the stability and identity of the magnetic carriers. Measurements were done on the Stanford University automated cryogenic magnetometer.

Stable magnetizations were isolated for more than 90% of the tonalite specimens during demagnetization. Tonalite specimens varied in natural remanent magnetization (NRM) intensity with a mean of 0.5 to 1.0 A/m and a high of 15 A/m. Specimens with low NRM intensities (generally less than 0.01 A/m) did not display stable demagnetization vectors. Thermal demagnetization showed that the stable components had unblocking temperatures that ranged from 250° to 570°C, although a few specimens maintained a consistent direction from NRM up to 700°C. Vector analysis was done with a computer-based vector-fitting program (7). Vectors were chosen only if they had at least four consecutive demagnetization steps lying in a 5°-radius cone about the best-fit vector. In cases where specimen cores from the same sample were analyzed by both AF and thermal demagnetization, the vectors obtained were within experimental error of each other. Within most individual sites, consistent directions could not be isolated, but when the remanence vectors from all sites were plotted, consistent patterns in direction became apparent. The apparent lack of consistency within sites may be due to the presence of several overprinting magnetizations that heterogeneously affected the Kaap Valley pluton, or to local remagnetization induced by lightning.

For analysis, the population of vectors was divided into two groups on the basis of pluton petrology. Sites in the hornblende tonalite at the pluton margin were assigned to group 1, and sites in the hornblende-biotite tonalite in the pluton interior were assigned to group 2. The data fell into several modes or clusters. Contoured stereograms of the remanence vectors (Fig. 2) showed that there are differences between

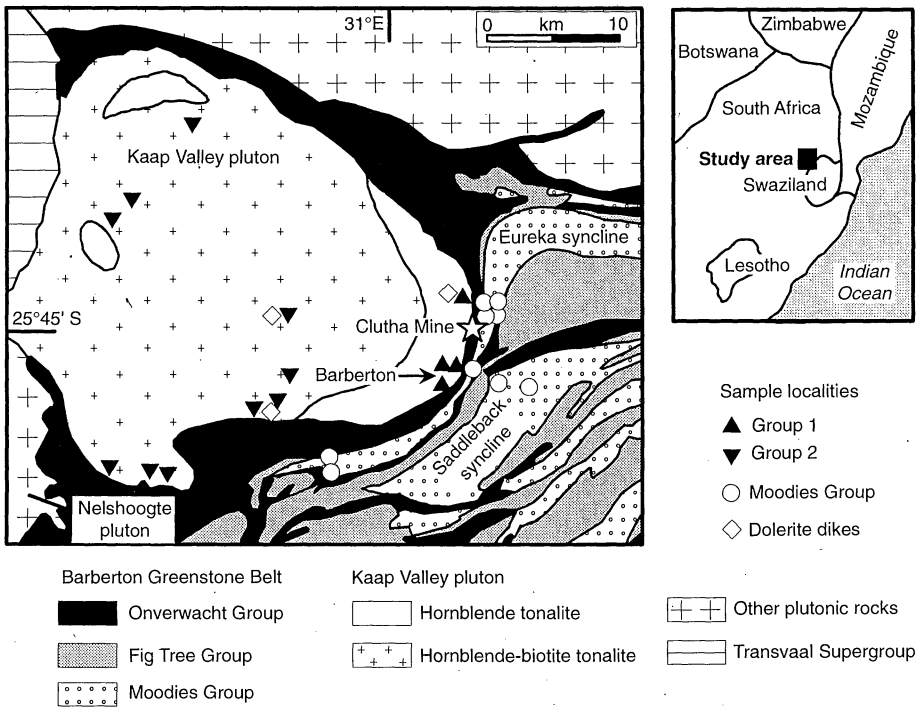

Fig. 1. Generalized geologic map of the Kaap Valley pluton showing the locations of the sampling localities for the paleomagnetic study [adapted from (2)]. Group 1 paleomagnetic sampling localities are from the hornblende tonalite phase of the pluton, and group 2 localities are from the hornblende-biotite phase. Localities are made up of more than one sampling site. The star is the location of the Clutha Gold Mine, and the arrow points to the location of the town of Barberton.

Table 1. Kaap Valley pluton paleomagnetic results. Modal analysis (8) was used to determine the characteristic directions of the data set. *N* is the total number of vectors used to identify the primary or secondary (denoted by an asterisk) mode for each group and polarity. For secondary modes in each group and polarity, *N* is reduced by the number of vectors associated with the primary mode. The best Fisherian (14) fit to the mode is the direction calculated from a subset of the data (*n* points). This is used to model the precision parameter (*k*) and the radius of the 95% confidence circle about the magnetic direction (β_{95}) of the mode. β_{95} is the error estimator for the mode and is identical to the α_{95} of the best Fisherian fit. Dec., magnetic declination; Inc., magnetic inclination; and deg, degree.

Group, mode, and polarity	Modal analysis			Best Fisherian fit to the mode				
	N	Dec. (deg)	Inc. (deg)	*n*	Dec. (deg)	Inc. (deg)	*k*	β_{95}
1 (B+)	66	354.1	78.9	20	357.3	79.2	27	6.4
1 (A+)	53*	252.2	64.3	10	251.6	63.5	76	5.6
2 (B+)	144	21.4	74.1	25	23.2	73.6	24	6.0
2 (A+)	113*	261.1	58.8	14	261.1	58.4	40	6.4
2 (A−)	97	40.2	−67.7	18	40.0	−67.4	48	5.1

*Secondary mode.

the two populations that may be due to either lithology or position in the pluton (margin compared with interior). The total number of vectors plotted (341) includes both primary remanence vectors (vectors that pass through the origin) and overprinting vectors, identified where two distinct vectors are seen in a specimen. For example, in one specimen from the pluton interior, a vector in mode C1 was seen overprinting mode A−. Other specimens from that site showed only the C1 direction, others showed the A− without an overprint, and still others showed "random" uncorrelated directions. We have chosen to treat all vectors (overprint and primary) equally in this analysis.

The most striking difference between the two populations is the lack of any significant grouping of negative inclination directions in group 1. This group shows only two positive inclination modes, A and B. Because the two directions are close to each other, it was difficult to assign vectors to either group for the purposes of statistical analysis. Modal analysis was used to identify these directions (*11*) (Table 1). The B mode is identical in direction to that from the dolerite dikes and from other early Proterozoic paleomagnetic poles (*9*–*11*) (Table 2), and we attribute this direction to Proterozoic overprinting of the tonalite. We interpret the A+ direction to be primary; that is, it was acquired when the pluton cooled.

Group 2 shows several directional modes with the positive inclination B mode as the most significant. The second most prominent mode is the negative inclination mode A−, antipodal to the A+ mode from group 1. Other significant modes in group 2 may be related to overprinting of the pluton by later intrusions. Mode C1 is similar in direction to the 3179-Ma Nelshoogte pluton (Fig. 1) that lies directly to the southwest of the Kaap Valley pluton (*3*, *12*), and mode C2 can be correlated with the magnetic direction of the 2875-Ma Usushwana Complex in Swaziland (*3*, *13*). Mode C3 has not been identified, although a similar direction is seen as an overprint in some dike samples, implying that it is younger than 2000 Ma. The A+ mode is also present in this group, although it is less pronounced than in group 1. It should be noted that the A+ and A− magnetization directions are never seen overprinting B+ or C directions. Because the margin of the pluton cooled through the magnetic blocking temperature before the interior, the pluton records a reversed to normal (in present coordinates) polarity transition. To separate "margin" and "interior" samples, we used the mapped petrologic divisions of hornblende tonalite and hornblende-biotite tonalite. It is possible that the cooling of the pluton through the magnetic blocking temperature did not follow this petrologic pattern such that some A+ vectors are seen in the interior and some A- vectors are seen at the pluton margin.

Shales of the Moodies Group were sampled in the area near the contact with the Kaap Valley pluton, in the Saddleback and Eureka synclines (Fig. 1). Sites were chosen with a wide dispersion of bedding orientation so that a fold test could be applied to the magnetic vectors obtained from the specimens. In 15 of 16 sites, a consistent magnetic direction (declination = 210°, inclination = 69°, α_{95} = 10°, where α_{95} is the radius of the 95% confidence circle around the mean direction) is seen. The Fisherian (*14*) precision parameter (k), a measure of the consistency of the orientation of the magnetic vectors, decreases from 17 to 4 when the beds are restored to paleohorizontal (with and without accounting for plunges of the synclines). This decrease in k indicates that the vectors are better grouped before restoration of the bedding to paleohorizontal, implying that the magnetization was acquired after folding of the beds. The direction of this magnetization is

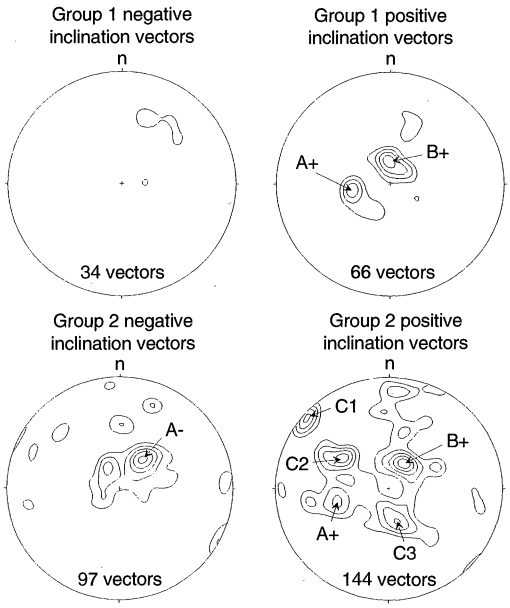

Fig. 2. Stereocontour plots of the magnetic vectors obtained from samples from the Kaap Valley pluton tonalite. For construction of these diagrams, all isolated magnetic vectors were plotted on stereonets (131 negative inclination vectors and 210 positive inclination vectors). Vectors are subdivided into groups 1 and 2 (see Fig. 1). Contour intervals are 2, 3, 4, 5, 6, 7, and 8 vectors per square degree of area on the net. Negative inclination vectors are plotted on an upper hemisphere equal-area projection, and positive vectors on a lower hemisphere projection. The modes listed in Table 1 are displayed. The other modes (C1, C2, and C3) are probably due to magnetic overprints caused by later intrusive events (*12*, *13*).

Table 2. Southern Africa Archean and Proterozoic paleomagnetic poles. A_{95} is the radius of the 95% confidence circle about the pole. For the Kaap Valley samples, g1 refers to group 1 and g2 to group 2. Lat., latitude; Long., Longitude.

Paleomagnetic pole	Lat. (°N)	Long. (°E)	A_{95} (deg)
Early Proterozoic (~2000 Ma)			
Kaap Valley B+ (g1)	5	30	6
Kaap Valley B+ (g2)	3	41	6
Dolerite dikes	17	44	24
Bushveld Complex (*12*)	16	30	4
Vredefort Ring (*13*)	28	34	11
Witwatersrand overprint (*14*)	19	46	8
Archean (3214 Ma)			
Kaap Valley A+ (g1)	−30	340	6
Kaap Valley A− (g2)	51	170	5
Moodies Group	−55	3	13

Table 3. Isotopic data from single-grain zircon evaporation. Sample BA33, a feldspar porphyry from the Clutha Mine (Fig. 1), was analyzed. Isotopic analyses were performed at the Max-Planck-Institut für Chemie in Mainz with a method described in (*15*). Mass scans are the number of $^{207}Pb/^{206}Pb$ ratios evaluated for age assessment. Mean $^{207}Pb/^{206}Pb$ is the observed mean ratio corrected for nonradiogenic Pb where necessary. The 2σ errors are based on uncertainties in the counting statistics.

Grain	Mass scans	Evaporation temperature (°C)	Mean $^{207}Pb/^{206}Pb$	Age (Ma)
1	98	1546	0.25636 ± 12	3224.5 ± 0.7
2	93	1528	0.25632 ± 15	3224.2 ± 0.9
3	66	1545	0.25647 ± 15	3225.2 ± 0.9
4	54	1520	0.25631 ± 16	3224.2 ± 1.0
Mean	306		0.25636 ± 7	3224.5 ± 0.4

close to the A+ direction obtained from the margin of the Kaap Valley pluton tonalite and reflects overprinting of the Moodies shale during pluton emplacement.

Zircon from a dike from the Clutha Mine (Fig. 1) that crosscuts the folded Moodies sediments has a single-grain Pb-Pb age of 3224.5 ± 0.4 Ma (Table 3), indicating that the Moodies was folded before this time. Because the A magnetization was acquired after folding, it is therefore only constrained to be younger than 3224 Ma and may coincide with the hornblende age of 3214 Ma.

Our paleomagnetic study of the Kaap Valley pluton shows two distinct magnetic directions. One is positive inclination that corresponds to an overprint direction caused by the intrusion of presumed early Proterozoic dikes and is seen in both the interior and margin of the pluton. The other direction is characterized by a negative inclination in the interior of the pluton (which is absent from the pluton margin) and an antipodal positive inclination in the margin of the pluton and in sediments adjacent to the pluton (which is present to a lesser degree in the pluton interior). This direction is significantly different from the present-day magnetic field direction and cannot be correlated with the timing of later thermal events that could have caused a magnetic overprinting. We believe this is a primary magnetization, acquired during cooling of the pluton at 3214 Ma. The data suggest that a reversal of Earth's magnetic field is preserved in the Kaap Valley pluton, making it the oldest observed reversal and implying that the reversing geomagnetic dynamo has been operating since the early Archean.

REFERENCES

1. M. W. McElhinny and W. E. Senanayake, *J. Geophys. Res.* **85**, 3523 (1980); C. J. Hale and D. J. Dunlop, *Geophys. Res. Lett.* **11**, 97 (1984).
2. P. W. Layer, A. Kröner, D. York, *Geology* **20**, 717 (1992).
3. A. Kröner and P. W. Layer, *Science* **256**, 1405 (1992).
4. E. S. Barton, W. Altermann, I. S. Williams, C. B. Smith, *Geology* **22**, 343 (1994).
5. L. J. Robb, J. M. Barton Jr., E. J. D. Kable, R. C. Wallace, *Precambrian Res.* **31**, 1 (1986).
6. A. R. Tegtmeyer and A. Kröner, *ibid.* **36**, 1 (1987); R. A. Armstrong, W. Compston, M. J. de Wit, I. S. Williams, *Earth Planet. Sci. Lett.* **101**, 90 (1990); S. L. Kamo, D. W. Davis, M. J. de Wit, *Geol. Soc. Aust. Abstr. Ser.* **23**, 53 (1990).
7. J. L. Kirschvink, *Geophys. J. R. Astron. Soc.* **62**, 699 (1980).
8. D. R. Van Alstine, *ibid.* **61**, 101 (1979).
9. P. J. Hattingh, thesis, University of Pretoria (1983).
10. R. B. Hargraves, *J. Geol.* **78**, 253 (1970).
11. P. W. Layer, A. Kröner, M. McWilliams, N. Clauer, *J. Geophys. Res.* **93**, 2191 (1988).
12. P. W. Layer, M. O. McWilliams, A. Kröner, *Eos* **45**, 689 (1983); P. W. Layer, A. Kröner, D. York, M. O. McWilliams, *ibid.* **70**, 1064 (1989).
13. P. W. Layer, A. Kröner, M. McWilliams A. Burghele, *J. Geophys. Res.* **93**, 449 (1988).
14. R. A. Fisher, *Proc. R. Soc. London Ser. A* **217**, 295 (1953).
15. A. Kröner, G. R. Byerly, D. R. Lowe, *Earth Planet. Sci. Lett.* **103**, 41 (1991).

25 March 1996; accepted 13 June 1996

Spectral Properties of Near-Earth Asteroids: Evidence for Sources of Ordinary Chondrite Meteorites

Richard P. Binzel, Schelte J. Bus, Thomas H. Burbine, Jessica M. Sunshine

Although ordinary chondrite (OC) meteorites dominate observed falls, the identification of near-Earth and main-belt asteroid sources has remained elusive. Telescopic measurements of 35 near-Earth asteroids (~3 kilometers in diameter) revealed six that have visible wavelength spectra similar to laboratory spectra of OC meteorites. Near-Earth asteroids were found to have spectral properties that span the range between the previously separated domains of OC meteorites and the most common (S class) asteroids, suggesting a link. This range of spectral properties could arise through a diversity of mineralogies and regolith particle sizes, as well as through a time-dependent surface weathering process.

Of the meteorites falling to Earth, 80% are stones consisting of olivine and pyroxene, which are classified as ordinary chondrites (OCs). They are thought to represent samples of the primitive solar nebula that have undergone modest thermal evolution over the age of the solar system (*1*). The most immediate sources for meteorites are likely to be near-Earth asteroids (*2*), which in turn are derived predominantly from the main asteroid belt (*3*). Relatively few spectroscopic observations of near-Earth asteroids have been obtained because of their small sizes, faint apparent magnitudes, and limited intervals of visibility. Of these measured asteroids, only one (1862 Apollo) has spectral properties widely recognized as similar to the laboratory spectral properties of OC meteorites (*4*–*6*). We now report the results of a survey of the visible-wavelength spectral properties of near-Earth asteroids: we find many that appear to have spectra similar to OC meteorites.

There has also been a long-standing debate over whether the most commonly observed (S class) asteroids are related to the most common meteorites, in spite of a mismatch in their red spectral slopes and absorption band depths. One hypothesis for this spectral mismatch is that some "space weathering" process is responsible for altering the spectral properties of OC asteroids (*7*). Another hypothesis is that Apollo-like OC asteroids (the Q class) exist as a population of small objects distinct from the S-class asteroids (*8*). Our observations do not reveal a distinct population of Q-class objects among small near-Earth asteroids.

We made spectroscopic measurements of 35 near-Earth asteroids, which we have obtained as target-of-opportunity observations over 1991 through 1996. In making these observations, we used a low-resolution spectrograph and solid-state charge-coupled device (CCD) detectors attached to the 2.4-m Hiltner telescope of the Michigan–Dartmouth–Massachusetts Institute of Technology (MDM) Observatory at Kitt Peak, Arizona (*9*). Our spectra cover the visible-wavelength range from 0.45 to 0.95 μm. Over these wavelengths, most of the asteroids categorized within the S class and most of the near-Earth asteroids we measured display spectra with a moderate absorption band near 1 μm, which arises owing to the presence of olivine and pyroxene (*10*, *11*). However, six of the near-Earth asteroids we measured have spectra that display unusually deep 1-μm absorption bands (Fig. 1). Over our measured wavelength range, the spectra of these near-Earth asteroids do not resemble 4 Vesta (Fig. 1A), but they do appear similar to the spectra of 349 Dembowska and 1862 Apollo (Fig. 1B) (*12*, *13*). Although Dembowska and Apollo clearly have distinguishable near-infrared spectra (*14*), such measurements for our set of faint near-Earth asteroids are not yet available. We make an inference for the spectra of our set of near-Earth asteroids by considering the mineralogies (based on near-infrared measurements) and meteorite analogs for Dembowska and Apollo. Dembowska is considered to be a pyroxene-olivine assem-

R. P. Binzel, S. J. Bus, T. H. Burbine, Department of Earth, Atmospheric, and Planetary Sciences, Massachusetts Institute of Technology, Cambridge, MA 02139, USA.
J. M. Sunshine, Department of Earth, Atmospheric, and Planetary Sciences, Massachusetts Institute of Technology, Cambridge, MA 02139, and Science Applications International Corporation, 4501 Daly Drive, Chantilly, VA 22021, USA.